Available online at www.sciencedirect.com
SCIENCE DIRECT®
Optics Communications 215 (2003) 367–379
OPTICS COMMUNICATIONS
www.elsevier.com/locate/optcom

Excitability and self-pulsations near homoclinic bifurcations in semiconductor laser systems

Bernd Krauskopf[a,*], Klaus Schneider[b], Jan Sieber[b], Sebastian Wieczorek[c], Matthias Wolfrum[b]

[a] *Department of Engineering Mathematics, University of Bristol, Bristol BS8 1TR, UK*
[b] *Weierstraß-Institut für angewandte Analysis und Stochastik, Mohrenstr. 39, D-10117 Berlin, Germany*
[c] *Physics and Astronomy, Vrije Universiteit Amsterdam, De Boelelaan 1081, 1081 HV Amsterdam, The Netherlands*

Received 1 July 2002; accepted 18 November 2002

Abstract

Many laser systems show self-pulsations with a large amplitude that are born suddenly in a homoclinic bifurcation. Just before the onset of these self-pulsations the laser is excitable where the excitability threshold is formed by the stable manifold of a saddle point. We show that there exists a special configuration, a codimension-two bifurcation called a non-central saddle-node homoclinic orbit, that acts as an organising centre of excitability in lasers. It is the key to understanding excitability in laser systems as diverse as lasers with saturable absorbers, lasers with optical injection and lasers with optical feedback.

PACS: 42.50.Ne; 42.55.Px; 05.45.+b

Keywords: Excitability; Self-pulsations; Semiconductor laser; Homoclinic bifurcation

1. Introduction

Excitability has been well known for a long time in physiology and chemistry. About half a century ago, the Nobel price winner Hodgkin [21] already described different kinds of neural excitability, namely a unique response to a stimulus above a certain threshold (all-or-none law) and repetitive firing to a sufficiently strong stimulus. The possibility of spontaneous firing is also well known [20]. Other examples of excitable physiological or chemical systems are neurons and axons [22,23], heart muscles [1,28], electrodissolution and passivation of iron [41], and different chemical reactions [25,26,34]. In recent years it has become clear that excitable systems are prevalent also in other fields of science, including population dynamics [4], protein dynamics (calcium waves) [44], and laser dynamics, the field we concentrate on here.

Recently, excitability in laser systems has been receiving considerable interest. It was found in nonlinear cavities with temperature dependent

* Corresponding author.
E-mail address: B.Krauskopf@bristol.ac.uk (B. Krauskopf).

0030-4018/02/$ - see front matter
PII: S0030-4018(02)02239-3

absorption [33], lasers with optical injection [48,54], lasers with optical feedback [37,57], multisection DFB lasers [56], lasers with integrated dispersive reflectors [50], and lasers with saturable absorber [7,8]; see also the overview [48]. This interest is also due to possible applications of excitability in lasers: the laser acts as an optical switch that reacts only to sufficiently high optical input signals. This may be used in optical communication systems, for example, for pulse reshaping (a dispersed input pulse can trigger a large 'clean' output pulse).

It is important to realise that the notion of excitability is defined phenomenologically. Following [39], a system is called *excitable* when:

(i) the unperturbed system is at a stable equilibrium;

(ii) a perturbation above the *excitability threshold* triggers a large excursion from the stable equilibrium;

(iii) the system then settles back to the attractor in what is called the *refractory phase*, after which the system can be excited again.

As we will see below, this large excursion can be quite complicated and produce not just a single pulse, but a fixed number of pulses.

When one models excitability in the framework of dynamical systems theory (e.g. by ordinary differential equations), then certain topological configurations of phase portraits are associated with different types of excitability [24,42,43]. An immediate question arises: how does the phase space have to be organised (apart from having a stable equilibrium) in order for a system to be excitable?

There are some known topological configurations of the phase space that imply excitability. One configuration represents a slow–fast system with an S-shaped slow manifold. This situation occurs in the FitzHugh–Nagumo model [13,38] (an approximation of the famous Hodgkin–Huxley equations [22] describing the action potential of a squid axon) as well as in a two-dimensional system modelling an optical cavity [33]. Another such configuration occurs in the original Hodgkin–Huxley equations [22]: there is a thin region in the phase space where the dynamics depend very sensitively on the initial conditions. This region can be interpreted as a threshold set [24] and indicates the existence of a quasi-threshold of excitability. This configuration also exists in a model of a laser with integrated dispersive reflectors [50].

In this paper we are concerned with yet another topological configuration that arises in models of excitable systems (see e.g. [42,43]), and in particular in models of laser systems; see the examples in Sections 3–5. The situation is sketched in Fig. 1: both branches of the one-dimensional unstable manifold of a saddle point end up at an attractor. This configuration comes in two cases or 'flavors': the unstable manifold of the saddle either forms a smooth invariant closed curve (Fig. 1(a)), or the two branches of the unstable manifold come back 'on the same side' of the attractor (Fig. 1(b)). In both cases (a) and (b), a small perturbation relaxes back to the attractor, while a perturbation beyond the stable manifold of the saddle results in a large excursion along one branch of the unstable manifold, and then a relaxation back to the attractor. The closer the saddle and the attractor are together, that is, the closer the system is to a saddle-node bifurcation, the 'more excitable' it is.

While there is no topological or qualitative difference between the two cases in Fig. 1(a) and (b), their distinction has a history that can be explained by the physical manifestation of the excitability associated with them. The excited pulse one gets when there is an attracting invariant circle is generally less sharp (in particular when there are several pairs of attractors and saddle points on the invariant circle [14]). For example, in an optically injected semiconductor laser one notices a 2π phase jump of the electric field with hardly a

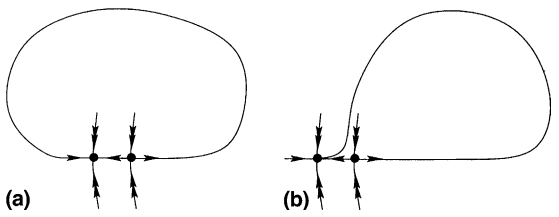

Fig. 1. Two 'flavors' of a topological configuration leading to excitability: the two branches of the unstable manifold of the saddle either form a smooth invariant closed curve (a), or they come back 'on the same side' of the attractor (b).

change in the laser intensity; see [52] and also Section 5. Case (b) on the other hand, can be characterised as being near a homoclinic bifurcation, and this typically leads to larger and shorter excitable pulses (and associated self-pulsations) in lasers; see Section 3. Indeed these changes are of a quantitative nature and depend on what observables can be measured in the system under consideration.

In this paper we emphasise the role of a nearby homoclinic orbit in both cases of Fig. 1 for understanding excitability in lasers. We identify a codimension-two bifurcation called a *non-central saddle-node homoclinic bifurcation* that acts as an organising centre for excitability. This special point ties together the cases (a) and (b) in a consistent way. We demonstrate with the examples of a laser with saturable absorber, a laser with optical feedback and an optically injected laser that excitability near homoclinic orbits is particularly prominent in lasers systems.

The paper is organised as follows. In Section 2 we discuss in more detail the phenomenon of excitability near a homoclinic orbit. Sections 3–5 discuss excitability in a laser with saturable absorber, with optical feedback and with optical injection, respectively. We draw some conclusions in Section 6.

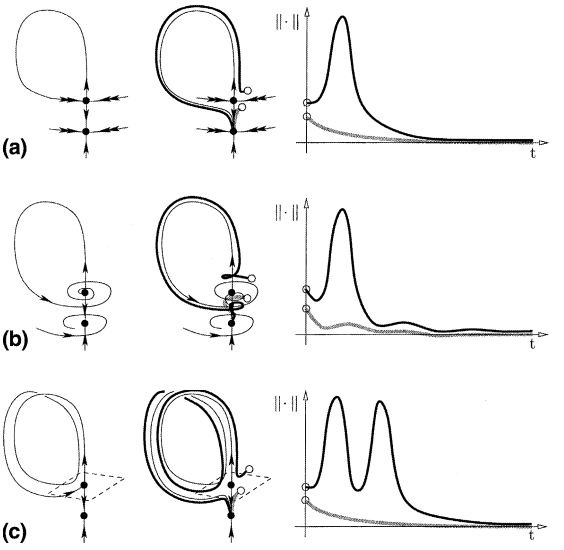

Fig. 2. Excitability near a homoclinic orbit to a real saddle (a), a homoclinic orbit to a saddle-focus (b), and a 2-homoclinic orbit (c). The respective homoclinic orbit is shown in the first column, the excitable phase portrait in the second column, and time traces in the third column. The last two columns show the reaction to a perturbation below (grey curves) and above (black curves) the excitability threshold.

2. Excitability near a homoclinic orbit

Three examples of excitability near a homoclinic orbit are sketched in Fig. 2. The respective homoclinic orbit itself is shown in the left column, the excitable phase portrait near the homoclinic orbit in the middle column, and time traces in the right column. It may be easiest to first consider the simplest situation of a homoclinic orbit in the plane as sketched in Fig. 2(a). While a small perturbation quickly relaxes back to the attracting equilibrium (grey curve), a perturbation above threshold, namely one above the stable manifold of the saddle, leads to a large excursion (black curve). During this excursion the system follows the unstable manifold of the saddle back to the equilibrium, which results in a pulse as is sketched in the right column. In Fig. 2(b) the saddle involved is a saddle-focus, so that the homoclinic orbit is of Shilnikov type. As a result, there is an element of oscillation in the reaction to perturbations, but otherwise the situation is exactly as in Fig. 2(a). Finally, Fig. 2(c) shows excitability near a so-called 2-homoclinic orbit where the unstable manifold misses the saddle at the first pass and connects to the saddle only when it comes close the second time. After a perturbation above threshold the system again follows the unstable manifold of the saddle. Because this manifold comes close to the saddle two times before ending up at the attractor, this now leads to two clearly discernible pulses as a result of *a single* perturbation above the excitability threshold. In general, there is an n-pulse reaction near an n-homoclinic orbit. We show in Section 5 that this effect, which we call *multipulse excitability*, is related to a Belyakov bifurcation [3] and actually occurs in an optically injected semiconductor laser.

There is an organising centre that allows us to describe different kinds of excitability and their

occurrence in lasers. It is a codimension-two bifurcation called a *non-central saddle-node homoclinic bifurcation*. At this special point, the unique part of the centre manifold of the saddle-node returns back to the saddle-node along the stable manifold of the saddle-node. Its unfolding (giving all possible dynamics near this point) is sketched in Fig. 3; see [2,24] for further details. The codimension-two point on the saddle-node curve S marks the transition from a saddle-node bifurcation *on an invariant closed curve* (formed by the unique part of the centre manifold of the saddle-node returning along the centre (linearly neutral) direction; phase portrait $1 \leftrightarrow 2$) to a saddle-node bifurcation *off an invariant closed curve* (a limit cycle; phase portrait $1 \leftrightarrow 4$). There is a homoclinic bifurcation curve h emanating from the codimension-two point, along which there is a homoclinic orbit to the saddle (phase portrait $3 \leftrightarrow 4$). It turns out that, to make this unfolding complete, there must be a curve *het* corresponding to a heteroclinic connection where the unstable manifold of the saddle returns to the attractor along the strong stable manifold (phase portrait $2 \leftrightarrow 3$). While this is not a bifurcation (phase portraits 2 and 3 are topologically equivalent; see also Fig. 1) this heteroclinic connection is the moment when the invariant closed curve is lost as a smooth object; see also [30]. We can now identify the region in parameter space where the system is excitable due to a saddle and an attractor on an invariant closed curve (Fig. 1(a)) as region 2, while it is excitable near a homoclinic orbit (Fig. 1(b)) in region 3. Both cases of excitability occur near the onset of self-pulsation, which one finds in regions 1 and 4. However, the boundary between self-pulsations and excitability is different in both cases. Importantly, in region 4 the selfpulsations co-exist with the attracting equilibrium.

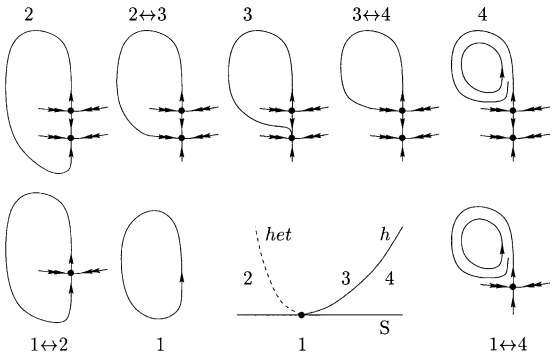

Fig. 3. Bifurcation structure near a non-central saddle-node homoclinic bifurcation point. Phase portrait 1 corresponds to self-pulsations, phase portrait 2 to excitability due to a saddle and an attractor on an invariant circle, phase portrait 3 to excitability near a homoclinic orbit, and phase portrait 4 to bistability between a steady state and self-pulsations.

Before considering examples in detail, we now discuss some practicalities of finding excitability in a given laser system.

It is an important question how one can experimentally achieve a sufficient perturbation to trigger a pulse. In lasers the triggering mechanism most used is a periodic train of short changes of the pump current [17]. Excitability then shows up as a corresponding train of optical pulses for sufficiently strong and sufficiently wide-spaced pulses [16,17,48]. From a dynamical systems point of view, this experimental technique is a change in a parameter and not a perturbation in phase space. One needs to be careful with the strength and duration of such a pulse in order to avoid the system simply adiabatically following this parameter change; see [50]. This is of particular importance for semiconductor lasers, which have very fast internal time scales. Only recently [56] the first experiment was conducted that used a small optical pulse, that is, a perturbation in phase space, to trigger an excited pulse.

Furthermore, many laser systems are only weakly dissipative. As a consequence, above the excitability threshold the size of the excited pulse varies somewhat with the size of the perturbation. This is in contrast with, for example, excitability in the FitzHugh–Nagumo system. This is why, in our characterisation of excitability above, we did not require the size of the output pulse to be independent of the input perturbation once excited, as some authors do; compare [48]. Nevertheless, this variation is much smaller than the noticeable and experimentally measurable difference of the reaction below and above the excitability threshold.

3. Laser with saturable absorber

One mechanism for self-pulsations in lasers (with absorbers) is called passive Q-switching. It is due to the interplay of the slowly responding population differences in a gain and an absorber medium and the much faster response of the electric field in the cavity. This type of oscillations is characterised by a slow build-up of carriers in the absorber which are then suddenly transformed into a short pulse of laser light, after which this process repeats. The result is a pulse train with a typical frequency of the order of several GHz; see for example [27,35].

Semiconductor laser diodes with saturable absorber are known both from experiments and numerical studies to show self-pulsations immediately after reaching their laser threshold [7]. Furthermore, they were recently shown to be excitable before threshold [8]. The basic dynamics of a laser with saturable absorber is modelled well by the Yamada model [58], a three-dimensional dynamical system given by the (dimensionless) equations

$$\begin{aligned} \dot{I} &= (G - Q - 1)I, \\ \dot{G} &= \gamma(A - G - GI), \\ \dot{Q} &= \gamma(B - Q - aQI), \end{aligned} \tag{1}$$

for the laser intensity I, the gain G, and the absorption Q. In Eq. (1) A is the bias current of the gain, B the amount of absorption, a the differential absorption relative to the differential gain, and γ the relative relaxation rate of gain and absorber. Because γ is small, typically of the order of 10^{-3}, Eq. (1) are a slow–fast system. The gain G and the absorption Q develop on the slow time scale, and the intensity I is the fast variable. It is an important feature of Eq. (1) that the plane $\{I = 0\}$ is invariant under the flow and a slow manifold at the same time.

There are two possible configurations of a semiconductor laser with saturable absorber: two segment lasers where the gain and absorber are spatially separated in the longitudinal direction, and stripe lasers where the absorber is constituted by the unpumped material next to the gain region. The Yamada model (1) is valid for both, provided that the decay times in gain and absorber are of the same order in the segment laser, or the diffusion between gain and absorber is negligible for the stripe laser.

Singular perturbation methods (making use of the limit of small γ) were applied to this system in [9,12,15] to obtain expressions for the pulse frequency and the maximum pulse intensity; see also [11]. A complete bifurcation analysis describing all possible dynamics of the model in dependence on all four parameters (that is, not only for small γ) was carried out in [7].

For the realistic values $B = 5.8$ and $a = 1.8$, the bifurcation diagram in the (A, γ)-plane is as shown in Fig. 4(a). The relevant phase portraits 1–4 that occur for small values of γ are sketched qualitatively. We remark that these phase portraits are presented as plots in a plane; the missing direction is always attracting. As the pump parameter A is increased for fixed small γ, the laser is initially off in regions 1 and 2, and then, after crossing its threshold given by the transcritical bifurcation T,

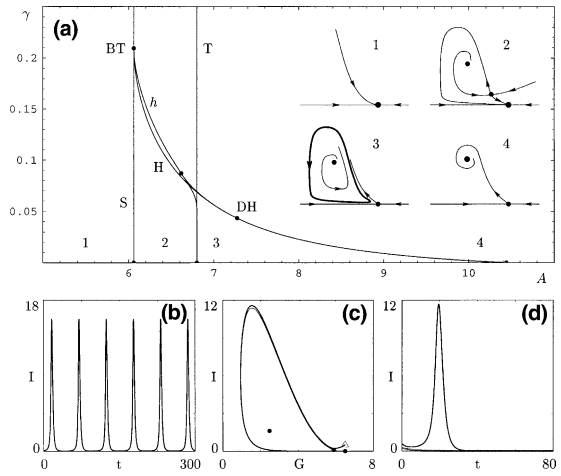

Fig. 4. The bifurcation diagram of the Yamada system in the (A, γ)-plane for $a = 1.8$ and $B = 5.8$ (a), together with the relevant phase portraits 1–4 for small γ. The laser shows self-pulsations (b) in region 3 ($A = 7.0$, $\gamma = 0.05$). It is excitable before the laser threshold in region 2 ($A = 6.5$, $\gamma = 0.05$) where a sufficiently strong excitation leads to a trajectory that follows closely the unstable manifold (almost entirely overdrawn thin curve) of the saddle (c). This leads to a single pulse in the intensity (black curve), while a sub-threshold perturbation immediately relaxes back to the off-solution (grey curve) (d).

produces pulse-like oscillations in region 3, as is shown in Fig. 4(b). These self-pulsations have been found in semiconductor lasers both in the stripe [36,47,58] and the longitudinal configuration [29]. They finally increase in frequency, become more sinusoidal and disappear in the Hopf bifurcation H. In region 4 the system is attracted to the single steady state with positive intensity, that is, the laser produces constant output.

In region 2, that is, just before threshold, the dynamics of the laser is topologically equivalent to Fig. 1(b) and therefore excitable. The excitability threshold is given by the two-dimensional stable manifold of the saddle closest to the off state (the attractor on the invariant plane $\{I = 0\}$). Because this saddle merges with the off state at the transcritical bifurcation T, which marks the laser threshold, the system is 'most excitable' just before the laser threshold. (The transcritical bifurcation plays the role of the saddle-node bifurcation in Sections 1 and 2 due to the invariance of $\{I = 0\}$.) A small perturbation simply relaxes back to the off state; see the grey curve in Fig. 4(d). However, Fig. 4(c) shows that a sufficiently large perturbation results in a trajectory that closely follows the one-dimensional unstable manifold of the saddle, resulting in a large pulse as is shown in Fig. 4(d). The system then relaxes back in a refractory phase along the slow manifold $\{I = 0\}$. In [8] it is shown that, once it is excited, the pulse has a height that depends linearly on the size of the perturbation. There one also finds an expression for the excitability threshold.

The excitability is due to the vicinity of the homoclinic orbit along the curve h, which emanates from a Bogdanov–Takens bifurcation BT. Even though the point BT lies in a part of the bifurcation diagram with unphysically large γ, it nevertheless acts as an organising centre for the dynamics [7]. The curve h was continued with AUTO/HomCont [6] from BT to values of small γ, which showed that the self-pulsations are indeed born in a homoclinic bifurcation as was conjectured, for example, in [9]. For small values of γ the curve h is virtually indistinguishable from the transcritical curve T, so that for all practical purposes the laser threshold coincides with this homoclinic bifurcation. This explains why the laser produces self-pulsations immediately after threshold.

Because noise is known to play an important role in self-pulsating lasers, we finish with some remarks on its effects on the dynamics of Eq. (1). This is the topic of [7], where the relevant equations and further details can be found. As can be seen in Fig. 4(a), the regions 1–4 in the bifurcation diagram are clearly separated by saddle-node, transcritical and Hopf bifurcations, respectively, in the physically relevant region of small γ (of the order of 10^{-3}). We found that this clear separation survives for realistic levels of spontaneous-emission noise. More importantly, in the excitable regime spontaneous-emission noise does not lead to a significant change in the excitability threshold and the pulse amplitude. On the other hand, much larger (externally injected) optical noise (of about 100 times the spontaneous-emission noise level) triggers a train of pulses before the laser reaches threshold. This pulse train displays minimal jitter for a particular level of the noise, an effect known as coherence resonance; see [7] for details.

4. Laser with optical feedback

Delayed optical feedback is known to be a source of instabilities and complicated dynamics in semiconductor lasers. In particular, the situation of large delay times has been studied extensively, both numerically and in experiments; see for example [5,40,46]. In this case, complicated dynamics with high-dimensional chaos is observed even for very small amounts of feedback. In contrast, the situation of an extremely short cavity, as it arises typically in multi-section devices with integrated cavity, has received less attention. (The external cavity of multi-section lasers is even much shorter than the short cavity regime investigated recently in [19].) However, this situation is of great practical interest as the small length of the external cavity makes the effects of delayed optical feedback much more controllable [56]. A detailed local bifurcation analysis in terms of the feedback phase ϕ and feedback strength η was performed in [10,46,55] for the well-known Lang–Kobayashi model [32] in the very short cavity regime.

The results of [10,46,55] locate the saddle-node curves and the curves of Hopf bifurcations of the stationary lasing states in the (ϕ,η)-plane. We will explore the (ϕ,η)-plane starting from small η, and search numerically for global bifurcations leading to the general scenario described in Sections 1 and 2. This implies excitability of the laser.

4.1. Lang–Kobayashi system

For our analysis, we model the laser-cavity system with the Lang–Kobayashi equations [32]. The scaling is appropriate for the case of a short cavity (see [55])

$$\begin{aligned}\dot{E}(t) &= (1+\mathrm{i}\alpha)n(t)E(t) + \eta \mathrm{e}^{-\mathrm{i}\phi}E(t-1),\\ \dot{n}(t) &= \varepsilon\Big[J - n(t) - (n(t)-v)|E(t)|^2\Big].\end{aligned} \tag{2}$$

Here the complex quantity E models the field amplitude, n describes the deviation of the carrier density from the laser threshold at $\eta = 0$, and time t is measured in multiples of the external round-trip time. As already mentioned, we choose the effective feedback strength η (which may be greater than 1 due to the rescaling of time) and the feedback phase ϕ as primary bifurcation parameters. The other parameters are the linewidth enhancement factor α, the ratio v between external and internal photon lifetime, the ratio ε between photon lifetime and averaged carrier lifetime, and J which models the pumping current.

Due to its rotational symmetry with respect to E, system (2) admits solutions of the type $E(t) = E_0\mathrm{e}^{\mathrm{i}\omega t}$, $n(t) = \text{const.}$, which are called stationary lasing states, external cavity modes or continuous-wave (CW) states.

4.2. Single-mode approximation

The factor ε in (2) is of order 10^{-2} if the length of the external cavity is of the same order as the length of the laser. This smallness of ε implies that the dimension of the dynamics of system (2) is low for a considerable range of η if all other parameters have a moderate magnitude; see for example [45,55]. We exploit this fact to reduce system (2) to a two-dimensional *single-mode approximation* [45,51] for small η.

Since we do not take into account nonlinear gain saturation, the equation for $\dot{E}$ in (2) is linear in E. We denote the corresponding linear operator by $H(n)$. The operator H acts on E as a function in the delay time interval. The characteristic function of $H(n)$,

$$\chi(\lambda;n,\eta,\phi) = \lambda - (1+\mathrm{i}\alpha)n - \eta\mathrm{e}^{-\mathrm{i}\phi-\lambda},$$

has only one complex root $\lambda \approx 0$ close to the imaginary axis in the vicinity of $n = 0$ and $\eta = 0$. That is, the compound cavity is in a single-mode regime for small η. We project E onto the eigenspace of $H(n)$ spanned by the dominant mode $\mathrm{e}^{\lambda t}$ using the corresponding adjoint eigenvector, and reduce the rotational symmetry of (2) to obtain an implicitly defined two-dimensional system of ordinary differential equations

$$\begin{aligned}\dot{I} &= \left(2\,\mathrm{Re}\,\lambda + \mathrm{Re}\left[\frac{(1+\mathrm{i}\alpha)(\lambda-(1+\mathrm{i}\alpha)n)}{(1+\lambda-(1+\mathrm{i}\alpha)n)^2}\right]\dot{n}\right)I,\\ \dot{n} &= \varepsilon(J - n - (n+v)I),\\ 0 &= h(\lambda;n,\eta,\phi),\end{aligned} \tag{3}$$

where $I = |E|^2$ and λ is the root of χ closest to the imaginary axis. According to [45,55], equilibria of (3) coincide exactly with CW states of system (2) and periodic orbits of (3) with moderate maximum power are $\sqrt{\varepsilon}$ close to self-pulsations of (2). Consequently, if the scenario described in Section 1 is present in system (3), we can conclude that the same scenario exists in (2) for parameters nearby.

4.3. Computational results

We fix the parameters $\alpha = 4$, $J = 2$, $v = 6$, and $\varepsilon = 0.01$ which correspond to the setting of a two-section laser investigated in [56] (consisting of an active single-mode laser section pumped well above threshold and a passive feedback section). We explore the (ϕ,η)-plane for $\eta \leqslant 0.5$ applying the standard numerical bifurcation analysis tool AUTO [6] to system (3). The parameter region of interest is depicted in Fig. 5(a). The region where the curve h of homoclinic orbits and the curve S of saddle-nodes join mirrors exactly the qualitative picture of Fig. 3. Moreover, it turns out that sys-

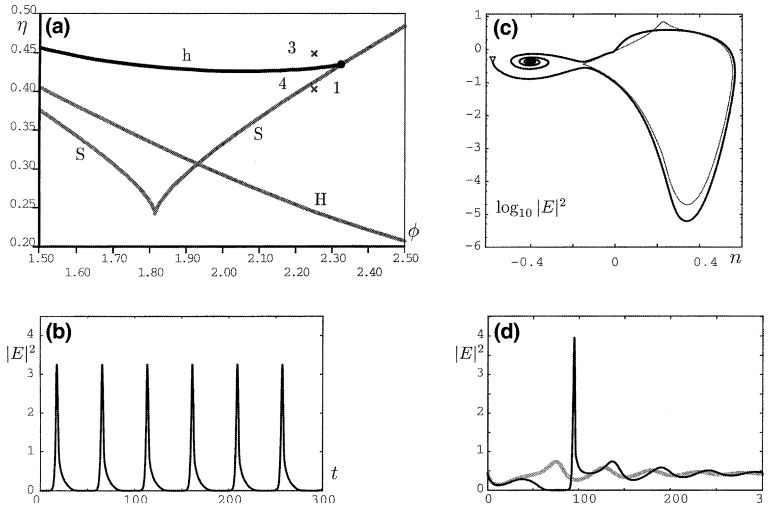

Fig. 5. Self-pulsations and excitability in the feedback laser near a non-central saddle-node homoclinic bifurcation point (a); also shown is a Hopf bifurcation curve H. The laser shows self-pulsations (b) in region 1 (cross at $\phi = 2.25$, $\eta = 0.4$). It is excitable in region 3 (cross at $\phi = 2.25$, $\eta = 0.447$) near the homoclinic bifurcation curve h, where a sufficiently strong excitation leads to a trajectory close to the homoclinic orbit (thin curve) (c). This leads to a single pulse in the intensity (black curve), while a sub-threshold perturbation relaxes back to the off-solution (grey curve) (d).

tem (2) behaves as the bifurcation diagram Fig. 5(a) of system (3) predicts. Fig. 5(b) shows that system (2) exhibits self-pulsations at the lower cross in Fig. 5(a) at $(\phi, \eta) = (2.25, 0.4)$. Fig. 5(c) and (d) display the excitable behavior of system (2) at the upper cross in Fig. 5(a) at $(\phi, \eta) = (2.25, 0.447)$. We excite the system by a sudden decrease of the carrier density n which is an approximate model for the injection of an incoherent optical pulse. The response of system (2) follows closely the shape of the nearby homoclinic orbit of system (3). There is one notable difference between the grey and the black curve in Fig. 5(c). The maximum power of the homoclinic of system (3) is too high compared to the maximum of the response of (2) (see Fig. 5(c)) due to a nearby singularity of the root λ of the characteristic function χ in system (3).

The response of system (2) to an excitation above its excitability threshold displays several characteristic features that are typical for a weakly dissipative system. Firstly, there is a noticeable delay before the pulse occurs (see Fig. 5(d), black time trace). During this delay, the carrier density increases continually until the pulse is emitted. Secondly, the rest state is a focus which is only weakly attracting. Finally, the maximum power of the pulse depends on the strength of the excitation because the attraction rate towards the unstable manifold of the saddle (guiding the response trajectory) is small.

Experimentally, excitability has been found in laser systems with delayed optical feedback in [48] in a double cavity ring laser. Moreover, [56] demonstrated for the first time excitability with respect to injected optical pulses using a multisection laser composed of a single-mode DFB laser and an integrated cavity. The small length of the integrated cavity ($\approx$250 μm) investigated in [56] enabled the experimentators to tune the phase ϕ of the feedback such that the system came close to a homoclinic bifurcation. However, the effective feedback strength η was chosen much higher than 0.5 in [56] leading to a genuine two-mode regime. This implied, for example, that the number of pulses of the response might depend on the strength of the excitation. However, the results depicted in Fig. 5 predict that excitability is essentially a single-mode phenomenon and should be observable also for an effective feedback strength η smaller than chosen in [56].

5. Laser with optical injection

The technique of optically (and unidirectionally) injecting the light of a master laser into a laser (today usually a semiconductor laser) results in a narrow linewidth when the laser locks onto the frequency of the master laser. Furthermore, by changing the frequency of the master, the frequency of the laser can be tuned. The main operational parameters are the injection strength K and the detuning ω between the frequency of the master laser and that of the free-running laser. It is intuitively clear that the laser will not lock onto the master laser for all combinations of injection strength and detuning, and indeed the injection laser is now known to show a wealth of additional behavior, especially when it is a semiconductor laser. We refer to [52] and further references therein as an entry point to the extensive literature.

An optically injected single-mode semiconductor laser is described well [53] by the rate equations

$$\begin{aligned} \dot{E} &= K + \left(\frac{1}{2}(1+\mathrm{i}\alpha)n - \mathrm{i}\omega\right)E, \\ \dot{n} &= -2\Gamma n - (1+2Bn)(|E|^2 - 1), \end{aligned} \tag{4}$$

for the complex electric field amplitude $E = E_x + \mathrm{i}E_y$ and the population inversion n. In Eq. (4) time is in units of the characteristic relaxation oscillation frequency ω_r of the free-running laser. As mentioned above, the two (experimental) control parameters are the injected field strength K and its detuning ω. Further, α is the linewidth enhancement factor, B the (rescaled) photon lifetime, and Γ the (rescaled) damping rate of the relaxation oscillations, which were set to the realistic values $\alpha = 2$, $B = 0.015$ and $\Gamma = 0.035$; see [52] for more details.

It was recently shown in [54] that the injection laser may show multipulse excitability, a multipulse response to a single perturbation, near n-homoclinic orbits. This phenomenon is explained here in more detail.

The parameter region of interest in the locking region for negative detuning ω is shown in Fig. 6(a). It was generally thought that in the injection laser the saddle-node bifurcation along the curve S always takes place on a periodic orbit (the continuation of the periodic orbit for $K = 0$ corresponding to the solitary laser). However, there is a homoclinic curve h^1 that forms a 'homoclinic tooth' and meets the saddle-node curve S at the two codimension-two non-central saddle-node homoclinic bifurcation points A_1 and A_2. The dynamics near A_1 and A_2 is as in Fig. 3: between A_1 and A_2 the saddle-node bifurcation at S does not take place on the basic periodic orbit (the one continued from the solitary laser solution), and we find (single-pulse) excitability near the homoclinic orbit along h^1. The unstable manifold in this excitability region is shown in Fig. 6(c) and the reaction to a perturbation in Fig. 6(g). A small perturbation dies out quickly (grey curve), whereas a sufficiently large perturbation (to above the stable manifold of the saddle) results in a single pulse before the laser settles back to the equilibrium (black curve).

However, there are many more homoclinic curves present in the region shown in Fig. 6(a), which is due to the two codimension-two Belyakov bifurcation points [3,18] B_1 and B_2. At these codimension-two points, the neutral saddle curve *ns* intersects h^1, meaning that the saddle-focus changes its type, so that above *ns* the homoclinic orbit on h^1 is no longer stable. Above *ns* we are in the situation of a chaotic Shilnikov bifurcation, near which one finds n-homoclinic orbits for any n (passing the saddle closely $(n-1)$ times before closing up); see for example [31]. The corresponding curves h^n lie inside the homoclinc tooth formed by h^1 and create a cascade of bifurcations that is not entirely understood yet [18]. Many of these curves of n-homoclinic orbits extend into the region below *ns*, leading to further Belyakov points when they cross *ns*. Below the curve *ns* the homoclinic bifurcations along h^n are non-chaotic Shilnikov bifurcations from which a single stable n-periodic orbit bifurcates. A good number of curves h^n get very close to the curve S or even 'attach' to it at further non-central saddle-node homoclinic bifurcation points. The complex array of homoclinic curves near S is shown in Fig. 6(b).

There are open regions bounded by curves h^n where the system reacts in a deterministic way by

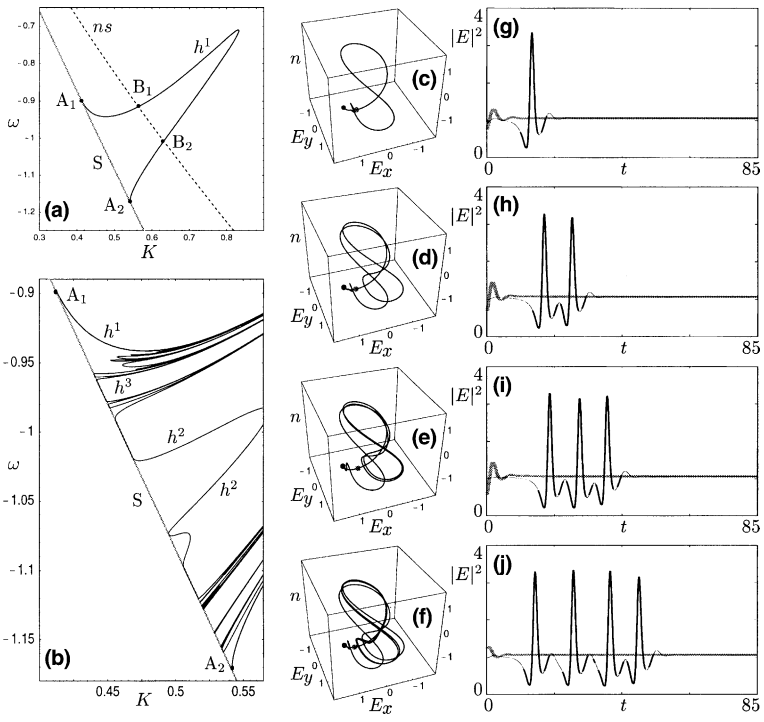

Fig. 6. Excitability in the injection laser near a curve h^1 of 1-homoclinic orbit connecting to the saddle-node curve S at two non-central homoclinic saddle-node points A_1 and A_2 (a). The curve h^1 is intersected by the neutral saddle curve *ns* at the Belyakov points B_1 and B_2, which implies the existence of curves h^n of *n*-homoclinic orbit for any *n*. Many of these *n*-homoclinic bifurcation curves also connect to S (b), and this leads to open regions where the system is multipulse excitable. In such a region a sufficiently strong excitation leads to a trajectory (c)–(f) that is close to the respective *n*-homoclinic orbit, resulting in an *n*-pulse in the intensity (black curve in (g)–(j)), while a small perturbation dies out (grey curve in (g)–(j)); time t is in units of ω_r. From (c)–(f) (K,ω) has the values: (0.45, −0.93), (0.472, −0.98), (0.48, −0.97), and (0.455, −0.95725).

producing an *n*-pulse to a sufficiently large perturbation. Several of these regions are so large that they should be experimentally accessible with todays experimental resolution of ≈ 100 MHz (ω is in units of $\omega_r \approx 5$ GHz); see [53]. The unstable manifolds in regions with 2-, 3- and 4-pulses are shown in Fig. 6(d)–(f). The respective reactions to a sub-threshold perturbation (grey curve) and to a sufficiently strong perturbation (black curve) are shown in Fig. 6(h)–(j). This is clear evidence of multipulse excitability in the injection laser.

It was generally believed that the locked solution is the only attractor in the locking region, although some indications of complex dynamics and period-doublings within the locking region were presented in [49]. Here we show that for values of (K,ω) inside the homoclinic tooth in Fig. 6(a), between S and *ns*, the laser may either lock to the input signal or show self-pulsations, which are due to additional attractors. Examples of such self-pulsations inside the locking region are shown in Fig. 7. Panels (a)–(c) show attractors in (E,n)-space, together with the attracting equilibrium corresponding to the locked state (black dot) and the saddle point (grey dot). Indeed, panels (a)–(c) are part of a period-doubling transition to chaos. The resulting chaotic attractor is shown in Fig. 7(c). The respective time series of the laser intensity are shown in panels (d)–(f), revealing characteristic self-pulsations. It is interesting to note that the amplitude of the self-pulsations practically does not change from (d)–(f), the only noticable difference being in the timing of the pulses. This is due to the shape of

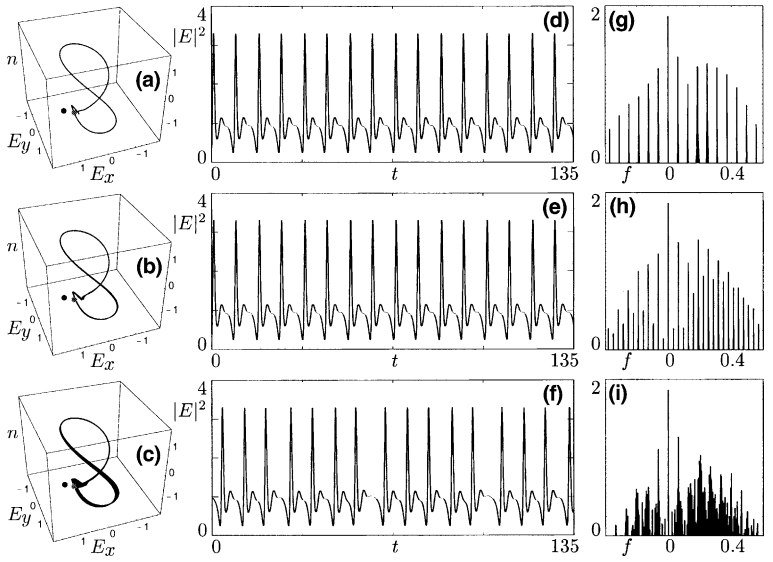

Fig. 7. Inside the locking region one finds a 1-periodic orbit (a), bifurcating to a 2-periodic orbit (b), and eventually to a chaotic attractor (c); the black dot represents the stable locked state and the gray dot the saddle equilibrium. The corresponding self-pulsations are shown in panels (d) and (e); time t is in units of ω_r. Notice that their amplitude hardly changes but the timing between consecutive pulses does, as is further evidenced in the respective optical spectra in panels (g)–(i); the frequency f is in units of $(\omega - \omega_{inj})/\omega_r$. From (a) to (c) $K = 0.445$ and ω is: -0.94, -0.942, and -0.9455.

the respective attractors in (E, n)-space. Even the chaotic attractor in Fig. 7(c) does not stray much from the first periodic orbit in panel (a). The clearest indication that we are indeed dealing with period-doubling to chaos comes from the optical spectra in panels (g)–(i), One clearly notices the extra peaks of the period doubled solution in panel (h), while panel (i) shows a continuous spectrum indicative of a chaotic attractor. Again, the chaotic nature is entirely in the timing of the pulses, leading to increased jitter.

The period-doubling curves involved in the cascade are not shown in Fig. 6(b). In fact, there is a complicated web of additional bifurcations, also including saddle-node bifurcations of periodic orbits, in the vicinity of the (infinitely many) Belyakov points. As was mentioned earlier, the exact nature of the bifurcation diagram near the Belyakov points is not known and beyond the scope of this paper. However, we found that, as is the case for the n-homoclinic curves h^n in Fig. 6(b), many of these additional bifurcation curves extend to near the saddle-node curve S, leading to extra attractors inside the locking region.

6. Discussion and conclusion

We gave a comprehensive survey of different occurrences of excitability in semiconductor lasers, taking a detailed look at lasers with saturable absorber, delayed optical feedback and optical injection. We discussed recent experimental and theoretical results and unveiled the common underlying mechanism: a non-central saddle-node homoclinic bifurcation, a codimension-two bifurcation, is the organising centre for excitability in laser systems. Hence, a careful bifurcation analysis of the theoretical models is the main tool for finding excitability. This analysis is the basis for the demonstration of excitability in the three different laser system in a unified manner. The fact that there is a common mechanism implies common features of these excitable systems, such as the slight dependence of the peak and the time of the excursion on the level of excitation (also above threshold) or the weak attraction of the rest state.

An important difference between the discussed configurations is the current state of their experimental verification. The phenomenon of

excitability itself has been demonstrated experimentally for a laser with optical injection [48] and multi-section DFB lasers with integrated cavity [56]. Fundamental characteristics, such as the refractory period or coherence resonance, have been studied only theoretically so far [8]. Corresponding experimental investigations on multi-section lasers are presently being conducted by Wünsche et al. [56]. Multipulse excitability in lasers with optical injection has not been verified experimentally yet. However, the excellent quantitative agreement between the overall bifurcation diagram and experimental measurements reported in [52] justify our expectation that such a verification might be achieved soon.

Acknowledgements

B. Krauskopf is supported by an EPSRC Advanced Research Fellowship and acknowledges hospitality and financial support from Weierstraß-Institut für angewandte Analysis und Stochastik. J. Sieber was supported by the Collaborative Research Centre 555 *Complex Nonlinear Processes* of the Deutsche Forschungsgemeinschaft. The research of S. Wieczorek was supported by the Foundation for Fundamental Research on Matter (FOM), which is financially supported by the Netherlands Organisation for Scientific Research (NWO).

References

[1] W.J. Adelman (Ed.), Biophysics and Physiology of Excitable Membrane, Van Nostrand–Reinhold, New York, 1971.
[2] F. Bai, A.R. Champneys, J. Dyn. Stab. Syst. 11 (1996) 327.
[3] L. Belyakov, Mat. Zam. 36 (1984) 838.
[4] D.R. Clother, J. Brindley, J. Math. Biol. 39 (1999) 377.
[5] R.L. Davidchack, Y.-C. Lai, A. Gavrielides, V. Kovanis, Physica D 145 (2000) 130.
[6] E. Doedel, T. Fairgrieve, B. Sandstede, A. Champneys, Yu. Kuznetsov, X. Wang, AUTO 97, http://indy.cs.concordia.ca/auto/main.html.
[7] J.L.A. Dubbeldam, B. Krauskopf, Opt. Commun. 159 (1999) 325.
[8] J.L.A. Dubbeldam, B. Krauskopf, D. Lenstra, Phys. Rev. E 60 (1999) 6580.
[9] T. Erneux, J. Opt. Soc. Am. B 5 (1988) 1063.
[10] T. Erneux, Proc. SPIE 3944 (2000) 588.
[11] T. Erneux, in: B. Krauskopf, D. Lenstra (Eds.), Multiple Time Scale Analysis of Lasers in Fundamental Issues of Nonlinear Laser Dynamics, AIP Conf. Proc., 548, AIP Melville, New York, 2000, p. 54.
[12] T. Erneux, P. Mandel, Z. Phys. B 44 (1981) 365.
[13] R. FitzHugh, Biophys. J. 1 (1961) 445.
[14] H. Gang, T. Ditzinger, C.Z. Ning, H. Haken, Phys. Rev. Lett. 71 (1993) 807.
[15] M. Georgiou, T. Erneux, Phys. Rev. A 45 (1992) 6636.
[16] G. Giacomelli, M. Guidici, S. Balle, J.R. Tredicce, Phys. Rev. Lett. 84 (2000) 3298, and private communication with J.R. Tredicce.
[17] M. Guidici, C. Green, G. Giacomelli, U. Nespolo, J.R. Tredicce, Phys. Rev. E 55 (1997) 6414.
[18] S.V. Gonchenko, D.V. Turaev, P. Gaspard, G. Nicolis, Nonlinearity 10 (1997) 409.
[19] T. Heil, I. Fischer, W. Elsäßer, A. Gavrielides, Phys. Rev. Lett. 87 (2001) 243901.
[20] H.-D. Henatsch, Z. Biol. 105 (1953) 17.
[21] A.L. Hodgkin, J. Physiol. 107 (1948) 165.
[22] A.L. Hodgkin, A.F. Huxley, J. Physiol. 117 (1952) 500.
[23] F.C. Hoppensteadt, An Introduction to the Mathematics of Neurons, Modeling in the frequency Domain, Cambridge University Press, Cambridge, 1997.
[24] E.M. Izhikevich, Int. J. Bifurc. Chaos 10 (2000) 1171.
[25] R. Kapral, K. Showalter (Eds.), Chemical Waves and Patterns, Kluwer, Academic Press, Dordrecht, 1995.
[26] H.R. Karfunkel, C. Kahlert, J. Math. Biol. 4 (1977) 183.
[27] H. Kawaguchi, Bistabilities and Nonlinearities in Laser Diodes, Artech House, Norwood, MA, 1994.
[28] J. Keener, J. Sneyd, Mathematical Physiology, Interdisciplinary Applied Mathematics, Springer, New York, 1998.
[29] R.G.M.P. Koumans, R. van Roijen, IEEE J. Quantum Electron. QE-32 (1994) 1122.
[30] B. Krauskopf, H.M. Osinga, in: E.J. Doedel, L.S. Tuckerman (Eds.), Numerical Methods for Bifurcation Problems and Large-Scale Dynamical Systems, IMA Volumes in Mathematics and its Applications, 119, Springer-Verlag, New York, 2000, p. 199.
[31] Yu.A. Kuznetsov, Elements of Applied Bifurcation Theory, Springer, New York, 1995.
[32] R. Lang, K. Kobayashi, IEEE J. Quantum Electron. 16 (1980) 347.
[33] W. Lu, D. Yu, R.G. Harrison, Phys. Rev. A 58 (1998) R809.
[34] R.-L. Luther, Z. Elektrochem. Angew. Phys. Chem. 12 (1906) 596.
[35] P. Mandel, Theoretical Problems in Cavity Nonlinear Optics Cambridge Studies in Modern Optics, Cambridge University Press, Cambridge, 1997.
[36] C.R. Mirasso, G.H.M. van Tartwijk, E.H. Garcia, D. Lenstra, P. Landais, P. Phelan, J. O'Gorgman, M. San Miguel, W. Elsäßer, IEEE J. Quantum Electron. 35 (1999) 764.
[37] J. Mullet, C.R. Mirasso, Phys. Rev. E 59 (1999) 5400.

[38] J.S. Nagumo, S. Arimoto, S. Yoshizawa, Proc. IRE 50 (1962) 2061.
[39] J.D. Murray, Mathematical Biology, Springer, Berlin, 1990.
[40] D. Pieroux, T. Erneux, T. Luzyanina, K. Engelborghs, Phys. Rev. E 63 (2001) 036211.
[41] D. Sazou, A. Karantonis, M. Pagitsas, Int. J. Bifurc. Chaos 3 (4) (1993) 981.
[42] K.R. Schneider, Monatsber. DAW 7 (1965) 671.
[43] K.R. Schneider, Monatsber. DAW 11 (1969) 451.
[44] J. Sneyd, St. Girard, D. Clapham, Bull. Math. Biol. 55 (1993) 315.
[45] J. Sieber, SIAM J. Appl. Dyn. Syst. 1 (2) (2002) 248.
[46] G.H.M. van Tartwijk, G.P. Agrawal, Prog. Quantum Electron. 22 (1998) 43.
[47] G.H.M. van Tartwijk, M. San Miguel, IEEE J. Quantum Electron. 32 (1996) 1191.
[48] J.R. Tredicce, in: B. Krauskopf, D. Lenstra (Eds.), Fundamental Issues of Nonlinear Laser Dynamics, AIP Conf. Proc., 548, AIP Melville, New York, 2000, p. 238.
[49] B. Tromborg, J. Mørk, IEEE J. Quantum Electron. 26 (4) (1990) 642.
[50] V.Z. Tronciu, H.-J. Wünsche, M. Radziunas, K.R. Schneider, Proc. SPIE 4283 (2001) 347.
[51] H. Wenzel, U. Bandelow, H.-J. Wünsche, J. Rehberg, IEEE J. Quantum Electron. 32 (1996) 69.
[52] S.M. Wieczorek, B. Krauskopf, D. Lenstra, Opt. Commun. 172 (1–6) (1999) 279.
[53] S.M. Wieczorek, T.B. Simpson, B. Krauskopf, D. Lenstra, Phys. Rev. E 65 (4) (2002) 045207(R).
[54] S.M. Wieczorek, B. Krauskopf, D. Lenstra, Phys. Rev. Lett. 88 (6) (2002) 063901.
[55] M. Wolfrum, D. Turaev, Opt. Commun. 212 (2002) 127.
[56] H.J. Wünsche, O. Brox, M. Radziunas, F. Henneberger, Phys. Rev. Lett. 88 (2002) 023901.
[57] A.M. Yacomotti, M.C. Eguia, J. Aliaga, O.E. Martinez, G.B. Mindlin, A. Lipsich, Phys. Rev. Lett. 83 (1999) 292.
[58] M. Yamada, IEEE J. Quantum Electron. 29 (1993) 1330.